https://dx.doi.org/10.4314/wojast.v15i2.25

SOME REMARKS ON THERMO-PHYSICAL PROPERTIES OF MAGNETOHYDRODYNAMICS HEAT AND MASS TRANSFER OF NANO-FLUID FLOW OVER A NONLINEAR PERMEABLE STRETCHING SHEET

ISSN: 2141 – 3290
www.wojast.com

EKANG, I. F.[1*] AND POPOOLA, A. O.[2]
[1]*Department of Mathematics, University of Uyo, Nigeria*
[2]*Department of Mathematical Sciences, Osun State University, Osogbo, Nigeria*
***Correspondence:** *idongesitekang@uniuyo.edu.ng*

ABSTRACT

The study aims to explore the potential benefits of investigating the MHD heat and mass transfer of nano-fluid over a nonlinear permeable stretching sheet. This is achieved by examining the influence of temperature-dependent viscosity and temperature-dependent thermal conductivity on nano-fluid. The governing partial differential equations that describe the nano-fluid flow are transformed and parameterized into a set of ordinary differential equations. These equations are subsequently solved numerically using shooting technique with the fourth order Runge-Kutta method. A graphical analysis is employed to assess the impact of specific fluid parameters on the momentum, thermal, and concentration equations. The outcomes depicted in the graphs reveal a noticeable effect of temperature-dependent viscosity and temperature-dependent thermal conductivity on the mathematical model.

KEYWORDS: Nano-fluid, MHD, temperature-dependent viscosity, temperature-dependent thermal conductivity

INTRODUCTION

In recent years, significant progress has been made in the field of magnetohydrodynamics (MHD) regarding heat and mass flow. One area of particular interest is the study of boundary layer flow over stretching sheets, which has proven to be essential in various technological applications. These applications include paper production, hot rolling, glass-fibre production, and extraction of polymer sheets.

Boundary layer behaviour on continuous solid surfaces were carried out by (Sakiadis, 1961), who made significant contributions to the understanding of continuous flow. (Crane, 1970) further analysed flow past a stretching plate. (Gupta and Gupta, 1977) explored heat and mass transfer on a stretching sheet with suction or blowing, employing the method of similar solutions. (Vajravelu, 2001) employed numerical methods to investigate viscous flow over a nonlinearly stretching sheet and established that heat always transfer from the stretching sheet to the fluid. (Wang, 2009) focused on studying analysis of viscous flow due to a stretching sheet with surface slip and suction.

Nano-fluids, characterised by the presence of nano-particles with sizes smaller than 100nm, play a significant role in various heat transfer applications. These applications encompass a wide range of industries, such as petroleum refining, pharmaceuticals, engine cooling, vehicle thermal management, chillers, fuel cells, domestic refrigerators, and grinding, to name a few. The base fluids commonly used in nano-fluids include water, ethylene glycol, and different oils derived from conventional mineral oils, crude oil and refined crude oil. Notably, nano-fluids exhibit distinct optical, electrical, and rheological properties that can be finely adjusted by manipulating the size, shape and concentration of the nano-particles.

(Khan and Pop, 2010) examined boundary layer flow of a nano-fluid past a stretching sheet. (Rana and Bhargava, 2012) investigated flow and heat transfer of a nano-fluid over a nonlinearly stretching sheet while (Das, 2015) extended this research by considering nano-fluid flow over a nonlinear permeable stretching sheet with partial slip, and his findings indicated that an increase in the slip parameter and nonlinear stretching parameter resulted in a decrease in the velocity of the nano-fluid. In a different study, (Ekang *et al.*, 2022) conducted an analysis on Casson fluid flow with heat generation and radiation effect through a porous medium of an exponentially shrinking sheet.

(Ayeni *et al.*, 2009)) conducted an examination into MHD flow and heat transfer of a viscous reacting fluid over a stretching sheet. (Eid and Mahny, 2017) focused on studying the unsteady MHD heat and mass transfer of a non-Newtonian nano-fluid flow of a two-phase model over a permeable stretching wall with heat generation/ absorption. (Popoola *et al.*, 2016) investigated heat and mass transfer on MHD viscoelastic fluid flow in the presence of thermal diffusion and chemical reaction. (Senge *et al.*, 2021) analysed influence of radiation on MHD flow over an exponentially stretching sheet embedded in a thermally stratified porous medium in the presence of heat source. (Oreyeni *et al.*, 2022) explained the significance of exponential space-based heat generation and variable thermo-physical properties on the dynamics of Casson fluid over a stratified surface with non-uniform thickness. Additionally, (Oreyeni *et al.*, 2022) studied triple stratification impacts on an inclined hydromagnetic bioconvective flow of micropolar nano-fluid with exponential space-based heat generation. (Ekang *et al.*, 2021) analysed MHD heat and mass flow of nano-fluid over a nonlinear permeable stretching sheet.

Temperature-dependent viscosity refers to the phenomenon where the viscosity of the fluid alters with temperature, impacting both flow behaviour and heat transfer rate. On the other hand, thermal conductivity denotes the material's capacity to conduct heat and can influence the rate of heat transfer within the system. By taking into account these factors, the study offers a more comprehensive and precise portrayal of the thermos-physical properties of the system, leading to a more realistic analysis.

This research aims at exploring the influence of temperature-dependent viscosity and temperature-dependent thermal conductivity on the findings of (Ekang *et al.*, 2021). The resulting system of ordinary differential equations was solved numerically by using the shooting method in conjunction with the fourth order Runge-Kutta method. The graphical representation of the results shows the impact of different fluid parameters on the momentum, thermal, and concentration distributions, allowing for a comprehensive analysis of their effects.

METHODS

Mathematical Formulation

In this study, we examined a two-dimensional and steady flow of an incompressible nano-fluid characterised by MHD heat and mass transfer. The flow takes place over a non-linear permeable stretching sheet aligned with the $y = 0$ plane. The coordinate system measures the distance normal to the surface of the stretching sheet in the vertical direction $y \geq 0$.

The flow is induced by a sheet emerging from a slit positioned at the origin ($x = y = 0$). The stretching velocity, denoted as u_w, exhibits a nonlinear variation as it depends on the distance from the slit. The non-linear variation is mathematically described by the equation $u_w = ax^n$, where a is a positive constant, n represents the nonlinear stretching parameter, and x is the coordinate measured along the surface.

The temperature of the sheet's surface is defined as:

$$T = T_\infty + (T_w - T_\infty) \text{ at } y = 0 \quad (1)$$

where T_∞ represents the ambient temperature, T_w is the temperature at the surface. The surface of the sheet is maintained at a constant concentration, denoted as C_w, where its value is assumed to be greater than the ambient concentration, represented by C_∞, and given as:

$$C = C_\infty + (C_w - C_\infty) \text{ at } y = 0 \quad (2)$$

The analysis incorporates the mathematical model considering the temperature-dependent viscosity and temperature-dependent thermal conductivity, given as:

$$\mu(T) = \mu^*(1 + \omega(T - T_\infty)) \text{ and } \quad k(T) = k^*(1 + \zeta(T - T_\infty)) \quad (3)$$

where $\omega, \zeta > 0$.

Under the assumption of a uniform magnetic field with strength B_o applied perpendicular to the stretching sheet at y > 0, the governing equations are given as:

$$\frac{\partial u}{\partial x} + \frac{\partial v}{\partial y} = 0 \quad (4)$$

$$u\frac{\partial u}{\partial x} + v\frac{\partial u}{\partial y} = \frac{1}{\rho}\left(\frac{\partial}{\partial x}\left(\mu(T)\frac{\partial u}{\partial y}\right) + \frac{\partial}{\partial y}\left(\mu(T)\frac{\partial u}{\partial y}\right)\right) - \frac{\sigma B_0^2}{\rho}u - \frac{\mu(T)}{\rho K}u \quad (5)$$

$$u\frac{\partial T}{\partial x} + v\frac{\partial T}{\partial y} = \frac{1}{\rho C_p}\left[\frac{\partial}{\partial x}\left(k(T)\frac{\partial T}{\partial x}\right) + \frac{\partial}{\partial y}\left(k(T)\frac{\partial T}{\partial y}\right)\right] + \tau\left[D_B\left(\frac{\partial C}{\partial x}\frac{\partial T}{\partial x} + \frac{\partial C}{\partial y}\frac{\partial T}{\partial y}\right) + \left(\frac{D_T}{T_\infty}\right)\left\{\left(\frac{\partial T}{\partial x}\right)^2 + \left(\frac{\partial T}{\partial y}\right)^2\right\}\right] \quad (6)$$

$$u\frac{\partial C}{\partial x} + v\frac{\partial C}{\partial y} = D_B\left(\frac{\partial^2 C}{\partial x^2} + \frac{\partial^2 C}{\partial y^2}\right) + \left(\frac{D_T}{T_\infty}\right)\left(\frac{\partial^2 T}{\partial x^2} + \frac{\partial^2 T}{\partial y^2}\right) \quad (7)$$

The relevant boundary conditions are as follows:

$$u = u_w + u_s,\ v = \pm v_w,\ T = T_w,\ C = C_w \quad \text{at } y = 0 \quad u \to 0,\ T \to T_\infty,\ C \to C_\infty \quad \text{as } y \to \infty \quad (8)$$

where u and v is the velocity components along the x- and y- axes, respectively, ϑ is the kinematic viscosity, μ is the dynamic viscosity, ρ is the fluid density, σ is the electrical conductivity, K is permeability of the porous medium, α is the thermal diffusivity, k is the thermal conductivity, c_p is the specific heat capacity, τ is the ratio between the effective heat capacity of the nano-particle material and heat capacity of the fluid, c is the volumetric volume expansion coefficient, ρ_f is the density of the base fluid, D_T is the thermophoretic diffusion coefficient, D_B is the Brownian diffusion coefficient, v_w denotes the suction/ injection velocity and u_s is the slip velocity which is assumed to be proportional to the local wall stress.

$$u_s = l\left(\frac{\partial u}{\partial x} + \frac{\partial u}{\partial y}\right)\Big|_{y=0} \quad (9)$$

The slip length, represented by l, acts as a proportional constant for the slip velocity.

The following transformation is employed to convert equations (5) to (7) into non-dimensional ordinary differential equations:

$$\psi = \left(\frac{2\vartheta a x^{n+1}}{n+1}\right) f(\eta), \qquad \eta = \left(\frac{a(n+1)x^{n-1}}{2\vartheta}\right)^{1/2} y,$$

$$u = ax^n f'(\eta)$$

$$v = -\left(\frac{\vartheta a(n+1)x^{n-1}}{2}\right)^{1/2}\left[f + \frac{(n-1)}{(n+1)}\eta f'\right],$$

$$T = T_\infty + (T_w - T_\infty)\theta(\eta), \quad \phi(\eta) = \frac{C - C_\infty}{C_w - C_\infty}$$

where ψ is the stream function defined as:

$$u = \frac{\partial \psi}{\partial y}, \qquad v = -\frac{\partial \psi}{\partial x}$$

The transformed ordinary differential equations obtained are as follows:

$$\left[\frac{[1+\gamma\theta][2Re(n+1) + (n-1)^2\eta^2]}{2Re(n+1)}\right] f''' + ff'' + \frac{(n-1)(5n-3)}{2(n+1)}\frac{1}{Re}\eta f'' - \frac{2n}{n+1}f'^2 + \frac{n(n-1)}{n+1}\frac{\gamma}{Re}\eta\theta' f' + \frac{(n-1)(5n-3)}{2(n+1)}\frac{\gamma}{Re}\eta\theta f'' + \gamma\left[\frac{2Re(n+1) + (n-1)^2\eta^2}{2Re(n+1)}\right]\theta' f'' + \frac{2}{n+1}\left[\frac{n(n-1)}{Re}(1 + \gamma\theta)\, Ha - La(1 + \gamma\theta)\right] f' = 0 \quad (10)$$

$$(1+\Omega\theta)\frac{1}{p_r}\left(\frac{(n-1)^2\eta^2+2(n+1)Re}{4}\right)\theta''+\frac{n+1}{2}Ref\theta'+(1+\Omega\theta)\frac{1}{p_r}\frac{(n-1)(n-3)}{4}\eta\theta'+\Omega\frac{1}{p_r}\left(\frac{(n-1)^2\eta^2+2(n+1)Re}{4}\right)\theta'^2+\left(\frac{(n-1)^2\eta^2+2(n+1)Re}{4}\right)Nb\phi'\theta'+\left(\frac{(n-1)^2\eta^2+2(n+1)Re}{4}\right)Nt\theta'^2=0 \quad (11)$$

$$\left[\frac{(n-1)^2\eta^2+2(n+1)Re}{4}\right]\phi''+\frac{n+1}{2}Scf\phi'+\frac{(n-1)(n-3)}{4}\eta\phi'+\frac{(n-1)(n-3)}{4}\frac{Nt}{Nb}\eta\theta'+\left[\frac{(n-1)^2\eta^2+2(n+1)Re}{4}\right]\frac{Nt}{Nb}\theta''=0 \quad (12)$$

The given boundary conditions are as follows:

$$f(\eta)=S,\ \ f'(\eta)=1+\xi f''(\eta),\ \ \theta(\eta)=1,\ \phi(\eta)=1 \quad \text{at} \quad \eta=0$$

$$f'(\eta)\to 0,\ \ \theta(\eta)\to 0,\ \ \ \phi(\eta)\to 0 \quad \text{as} \quad \eta\to\infty \quad (13)$$

The skin friction coefficient, C_f, the local Nusselt number, Nu_x, and the Sherwood number, Sh_x, are the primary physical quantities of interest. These quantities are defined as follows:

$$C_f=\frac{\tau_w}{\rho u_w^2},\quad Nu_x=\frac{xq_w}{k_1(T_w-T_\infty)},\qquad Sh_x=\frac{xJ_w}{D_B(C_w-C_\infty)} \quad (14)$$

where $\tau_w=\mu(\frac{\partial u}{\partial y})_{y=0}$ is the surface shear stress, $q_w=-k(\frac{\partial T}{\partial y})_{y=0}$ is the heat flux,

$J_w=-D_B(\frac{\partial C}{\partial y})_{y=0}$ is the wall mass flux, μ is the dynamic viscosity and k is the thermal conductivity. By the utilization of similarity variables, we can express these as:

$$Re_x^{1/2}C_f=(\frac{n+1}{2})^{1/2}f''(0),\quad Re_x^{-1/2}Nu_x=-(\frac{n+1}{2})^{1/2}\theta'(0),\quad Re_x^{-1/2}Sh_x=-(\frac{n+1}{2})^{1/2}\phi'(0) \quad (15)$$

The following variables are defined as follows: $Re=\frac{xu_w}{\vartheta}$ is the Reynolds number, $Ha=\frac{x\sigma B_0^2}{u_w\rho}$ is the Hartmann parameter, $La=\frac{x\vartheta}{u_wK}$ is the Permeability parameter, Pr $=\frac{\vartheta}{\alpha}$ is the Prandtl number, $Sc=\frac{u_wx}{D_B}$ is the Schmidt number, $Nb=\frac{\tau D_B(C_w-C_\infty)}{\vartheta}$ is the Brownian motion parameter, $\gamma=\omega(T_w-T_\infty)$ is the temperature-dependent viscosity, $\Omega=\zeta(T_w-T_\infty)$ is the temperature-dependent thermal conductivity, $Nt=\frac{\tau D_T}{\vartheta T_\infty}(T_w-T_\infty)$ is the thermophoresis parameter, $S=-\frac{v_w}{(\frac{a\vartheta(n+1)x^{n-1}}{2})^{1/2}}$ is the suction/ injection parameter and $\xi=l(\frac{a(n+1)x^{n-1}}{2\vartheta})^{1/2}$ is the slip parameter for liquids.

Method of Solution

In order to solve the dimensionless governing equations (10), (11) and (12) with their corresponding boundary conditions (13), we utilise a combination of the shooting method and the fourth order Runge-Kutta technique. To start, we introduce new variables for the equations as follows:

$$f_1=\eta,\ f_2=f,\ f_3=f',\ f_4=f'',\ f_5=\theta,\ f_6=\theta',\ f_7=\phi,\ f_8=\phi' \quad (16)$$

The system of coupled higher order nonlinear differential equations (10), (11), and (12) along with the boundary conditions (13), governing the system in its dimensionless form, are transformed into a set of first order differential equations. Following the standard practice in boundary layer analysis, the boundary conditions are adjusted by substituting the conditions at $\eta\to\infty$ with a finite value.

$$f_1{}'=1$$

$$f_2{}'=f_3$$

$$f_3{}'=f_4$$

$$f_4'=\Big(\frac{2Re(n+1)}{[1+\gamma\theta][2Re(n+1)+(n-1)^2\eta^2]}\Big)\Big(-ff''-\frac{(n-1)(5n-3)}{2(n+1)}\frac{1}{Re}\eta f''+\frac{2n}{n+1}f'^2-\frac{n(n-1)}{n+1}\frac{\gamma}{Re}\eta\theta'f'-\frac{(n-1)(5n-3)}{2(n+1)}\frac{\gamma}{Re}\eta\theta f''-\gamma\left[\frac{2Re(n+1)+(n-1)^2\eta^2}{2Re(n+1)}\right]\theta'f''-\frac{2}{n+1}\left[\frac{n(n-1)}{Re}(1+\gamma\theta)-Ha-La(1+\gamma\theta)\right]f'\Big)$$

$$f_5{}'=f_6 \quad (17)$$

$$f_6' = \left(\frac{4Pr}{[1+\Omega\theta][(n-1)^2\eta^2+2(n+1)Re]}\right)\left(-\frac{n+1}{2}Ref\theta' - [1+\Omega\theta]\frac{1}{p_r}\frac{(n-1)(n-3)}{4}\eta\theta' - \frac{\Omega}{p_r}\left[\frac{(n-1)^2\eta^2+2(n+1)Re}{4}\right]\theta'^2 - \left[\frac{(n-1)^2\eta^2+2(n+1)Re}{4}\right]Nb\phi'\theta' - \left[\frac{(n-1)^2\eta^2+2(n+1)Re}{4}\right]Nt\theta'^2\right)$$

$$f_7' = f_8$$

$$f_8' = \left(\frac{4}{(n-1)^2\eta^2+2(n+1)Re}\right)\left(-\frac{n+1}{2}Scf\phi' - \frac{(n-1)(n-3)}{4}\eta\phi' - \frac{(n-1)(n-3)}{4}\frac{Nt}{Nb}\eta\theta' - \left[\frac{(n-1)^2\eta^2+2(n+1)Re}{4}\right]\frac{Nt}{Nb}\theta''\right)$$

In the analysis, the notation of primes denotes differentiation with respect to η. We begin by making guesses for the values of $f''(0)$, $\theta'(0)$, and $\phi'(0)$ to ensure equation (13) is satisfied. To validate the numerical method used in this work, the nano-particles concentration profile result was compared with those of Ekang *et al*. (2021) for parameters at $n = 2, S = 0.2$, $Re = 1$, $Ha = 1$, $La = 1$, $Sc = 5$, $Nb = 0.5$, $Nt = 0.5$, $Pr = 2$, $G = \gamma = 0$, $\Omega = Ohm = 0$. The comparison is displayed in figure 1.

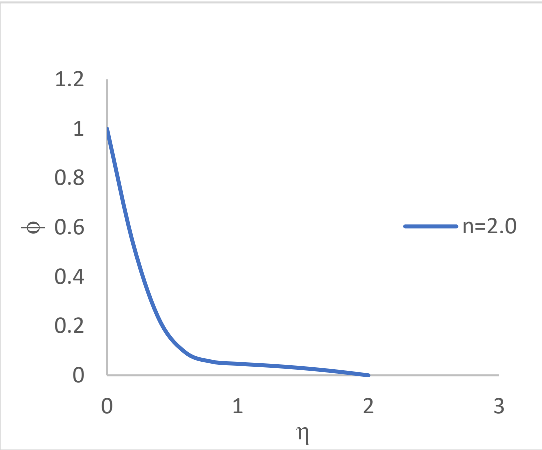

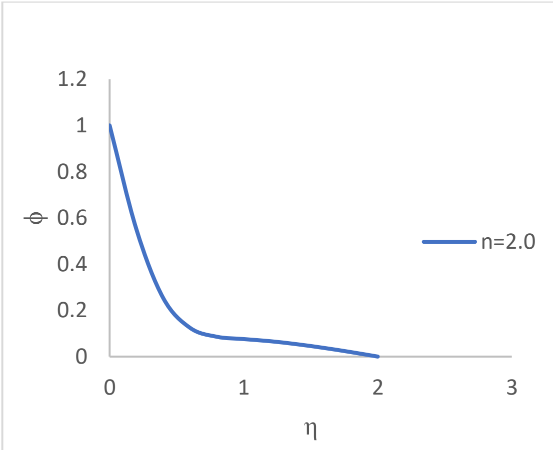

Fig. 1: (a) Present work (b) Ekang *et al*, 2021 work

The obtained results are then presented using tables and graphs, which are subsequently analysed and discussed to emphasise their significant characteristics.

RESULTS AND DISCUSSION

The notable impacts of fluid factors such as temperature-dependent viscosity, temperature-dependent thermal conductivity, nonlinear stretching parameter, magnetic field parameter, permeability parameter, Brownian motion parameter, thermophoresis parameter, Prandtl number, Lewis number on velocity, temperature and nano-particle concentration profiles are examined numerically using the shooting method. Numerical values obtained were plotted on graphs, where the fluid parameters were varied with basic at $n = 2$, $S = 0.2$, $Re = 1$, $Ha = 1$, $La = 1$, $Sc = 5$, $Nb = 0.5$, $Nt = 0.5$, $Pr = 2$, $G = \gamma = 1$, $\Omega = Ohm = 1$.

Figure 2 illustrates the impact of temperature-dependent viscosity on $f'(\eta)$. Increasing the temperature-dependent viscosity corresponds to an increase in the $f'(\eta)$ of the fluid. With rising fluid temperature, the viscosity decreases, resulting in reduced internal friction. As a result, the fluid flows more smoothly and at a higher velocity.

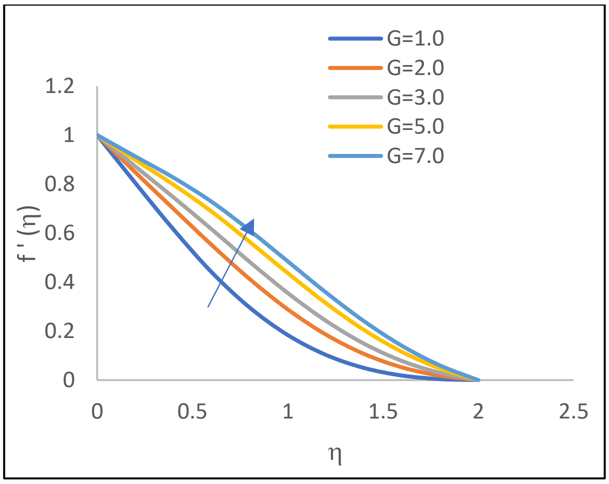

Fig. 2: comparing G on velocity profiles

Figure 3 shows the effect of temperature-dependent thermal conductivity on the $\theta(\eta)$ of the fluid.

A rise in temperature-dependent thermal conductivity has a notable influence on the temperature profiles. The fluid's thermal conductivity varies with temperature, thereby affecting its flow behaviour. Increased thermal conductivity facilitates the flow of heat within the fluid, leading to a higher temperature gradient.

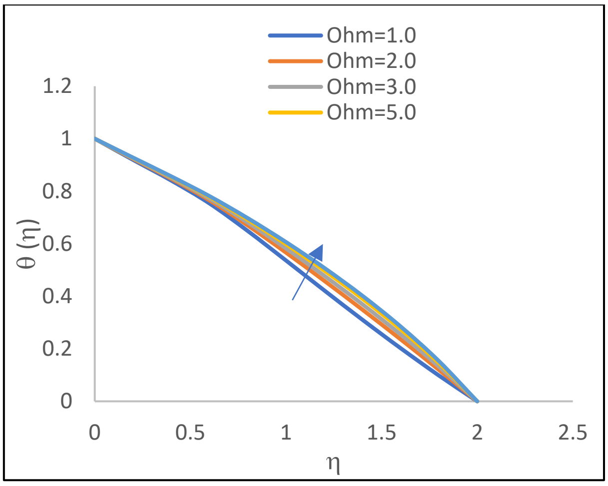

Fig. 3: comparing Ohm on temperature profiles

Figures 4, 5 and 6 depict the effect of the nonlinear stretching parameter on the $f'(\eta)$, $\theta(\eta)$, $\phi(\eta)$of the fluid. The velocity profiles are affected by an increase in the values of the nonlinear stretching parameter. The stretching parameter characterises the level of nonlinearity in the stretching of the sheet and a higher stretching parameter indicates a more pronounced stretching effect. This, in turns, results in the acceleration of the fluid to accelerate and an increased flow velocity.

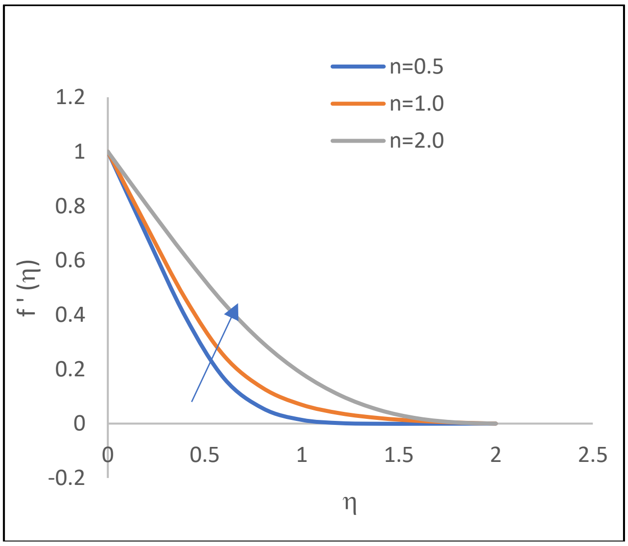

Fig. 4: comparing n on velocity profiles

The temperature profiles are significantly influenced by an increase in the values of the nonlinear stretching parameter. The stretching parameter quantifies the degree of stretching applied to the fluid which affect its flow behaviour of the fluid and also leads to an increase in temperature distribution of the system.

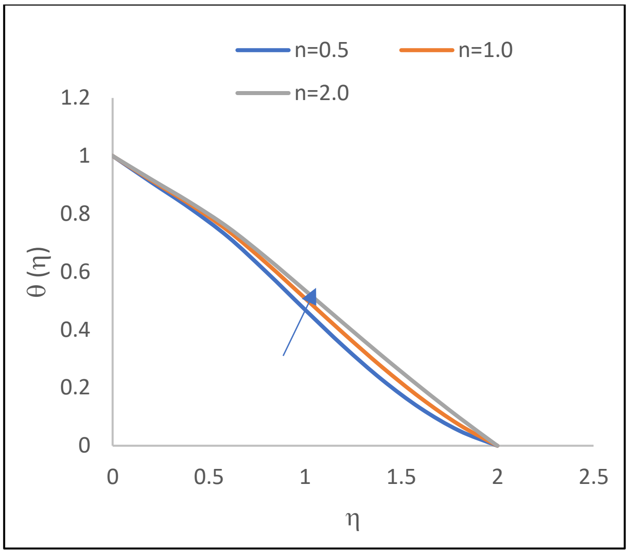

Fig. 5: comparing n on temperature profiles

An increase in the nonlinear stretching results to an increase in the concentration profiles of nano-particles. The nonlinear stretching parameter describes the rate at which the stretching surface increases in size along a particular direction. An increase in the nonlinear stretching parameter results in a faster increase in the size of the stretching surface, which in turn lead to an increase in the concentration of nano-particles in the fluid near the stretching surface.

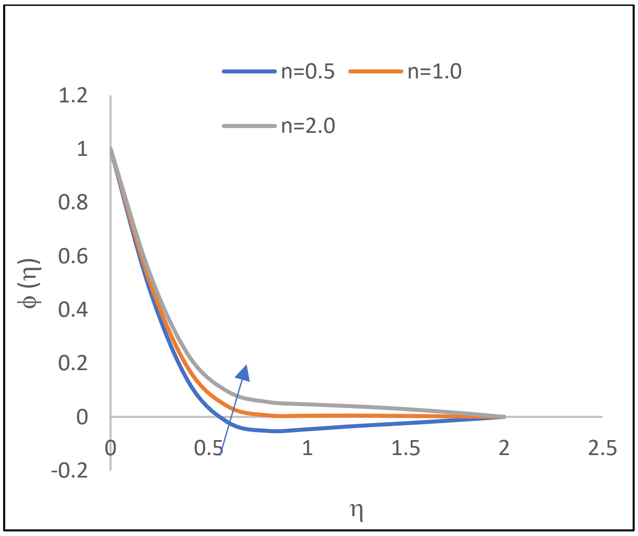

Fig. 6: comparing n on nano-particle concentration profiles

Figures 7 show how the $f'(\eta)$ of the fluid are affected by the magnetic field parameter. The velocity profiles are influence by an increase in the values of magnetic field parameter. The magnetic field parameter indicates the strength of the applied magnetic field, and a higher magnetic field parameter corresponds a stronger magnetic field affect. The stronger magnetic field generate a magnetic Lorentz force that opposes the fluid motion resulting in a reduction in velocity profiles.

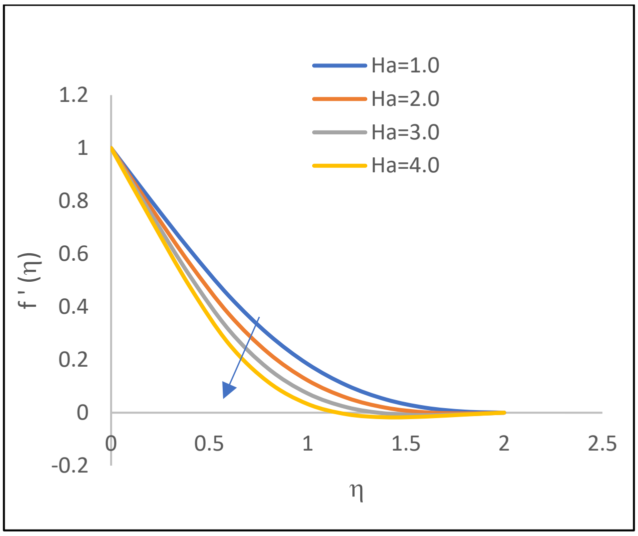

Fig. 7: comparing Ha on velocity profiles

Fig. 8 illustrate how the permeability parameter affects the $f'(\eta)$ of the fluid. An increase in the values of the permeability parameter affects the velocity profiles. The permeability parameter describes the degree of permeability of the stretching sheet, and a higher permeability depicts a higher degree of permeability which increases the drag force on the fluid and in turn reduce the fluid velocity.

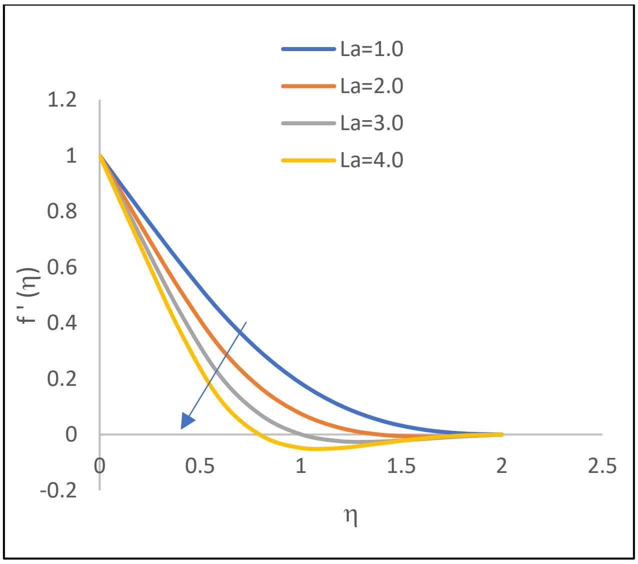

Fig. 8: comparing La on velocity profiles

Figures 9 and 10 depicts how the $\theta(\eta)$ and $\phi(\eta)$ is affected by the Brownian motion parameter of the fluid. The Brownian motion parameter signifies the effect of random thermal motion on the nano-particles suspended in the base fluid. An increase in the Brownian motion parameters corresponds to an increase in the random motion of the nano-particles which results in an increase in their collision frequency with the fluid molecules. This increased frequency result in enhanced heat transfer between the nano-particles and the fluid, leading to an increase in the temperature profiles.

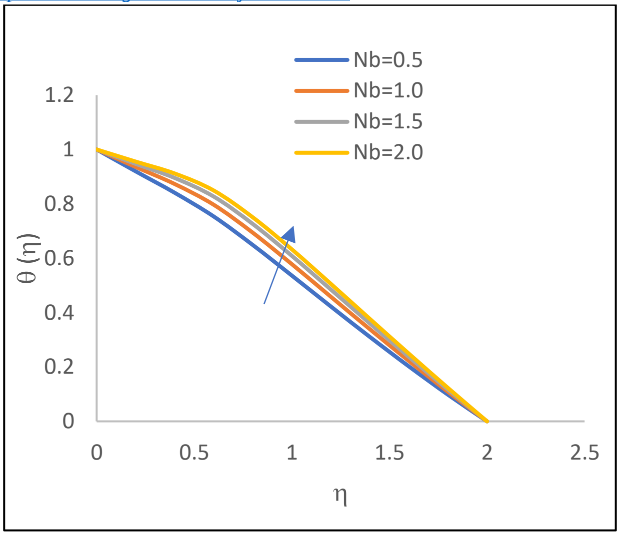

Fig. 9: comparing Nb on temperature profiles

As the Brownian motion parameter increases, the particles experiences more random motion, leading to their dispersion in the fluid. Consequently, the concentration profiles of the nano-particles decrease as they become more dispersed throughout the fluid.

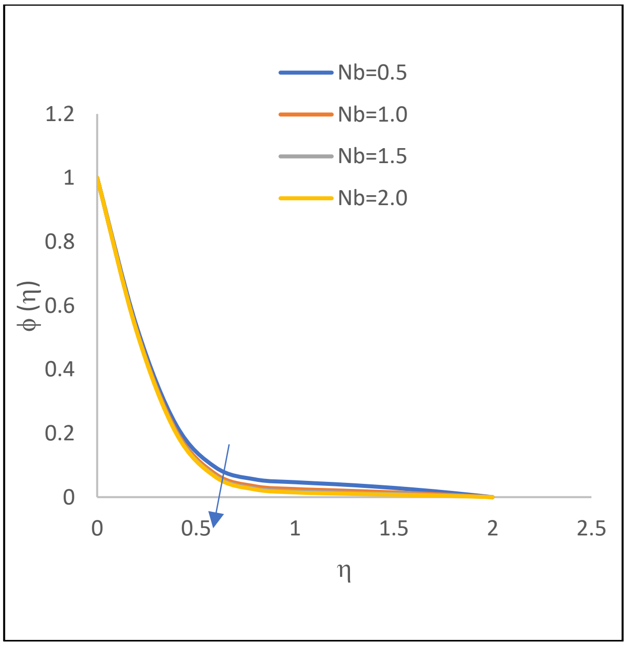

Fig. 10: comparing Nb on nano-particle concentration profiles

Figures 11 and 12 highlight the effect of thermophoresis parameter on the $\theta(\eta)$ and $\phi(\eta)$ of the fluid. The temperature is observed to rise as the thermophoresis parameters increase. Thermophoresis parameter contributes to increase in the thermal boundary layer thickness and leads to elevated surface temperatures on the sheet. This is because the thermophoresis parameter is directly proportional to the heat transfer coefficient associated with the fluid.

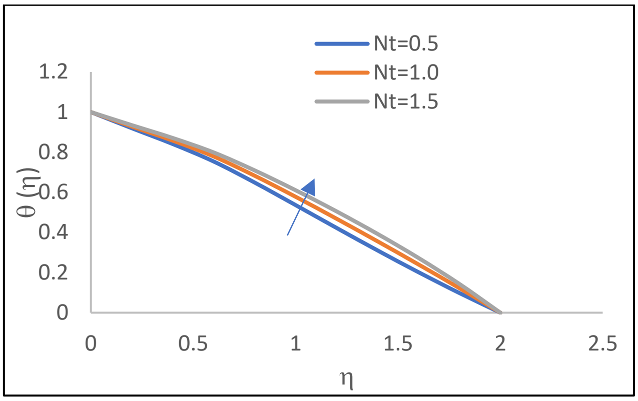

Fig. 11: comparing Nt on temperature profiles

The concentration profiles are seen to increase with increasing values of thermophoresis parameters. Concentration is an increasing function of thermophoresis parameter. This is due to the fact that nano-particles tend to migrate towards region of higher temperature, leading to an increase in the nano-particle concentration profiles.

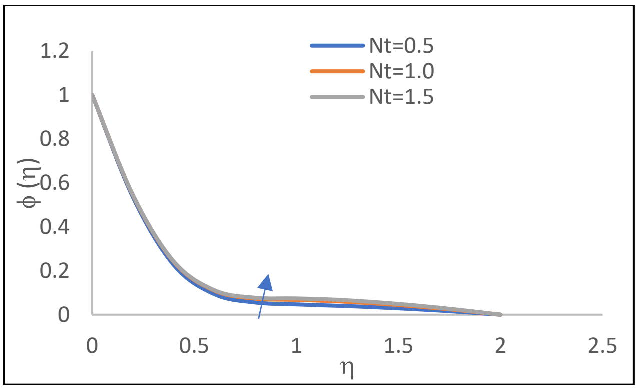

Fig. 12: comparing Nt on nano-particle concentration profiles

Figures 13 represents the $\theta(\eta)$, for various values of Prandtl numbers of the fluid. An increase in the Prandtl numbers results to an increase in the ratio of thermal diffusivity to momentum diffusivity, indicating that the fluid is less efficient at transferring heat compared to momentum. A higher Prandtl number indicates that the fluid is less efficient at transferring heat, which result in a lower temperature gradient in the system.

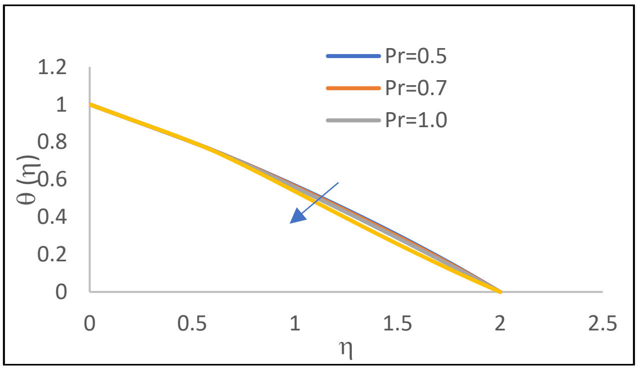

Fig. 13: comparing Pr on temperature profiles

Figure 14 manifest the Schmidt number on the $\phi(\eta)$ of the fluid. A higher Schmidt number indicates that thermal diffusivity is greater than mass diffusivity which shows that the rate of heat transfer in the fluid is higher compared to the rate of mass transfer. As a result, the temperature of the fluid increases faster than the concentration of the nano-particles resulting to a decrease in the concentration profiles of the nano-particles. Thermal energy in the fluid is transferred more easily than the nano-particles due to the difference in their diffusivities.

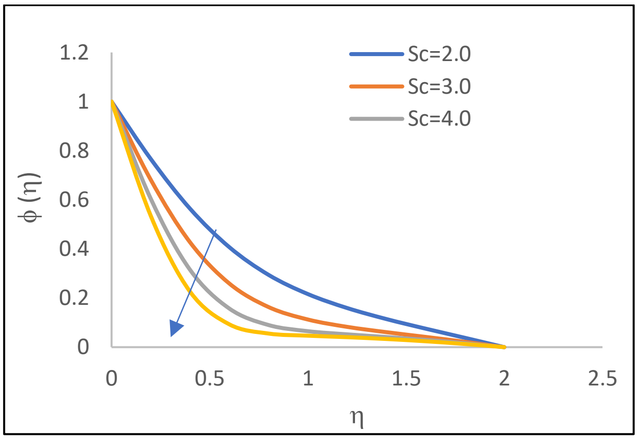

Fig. 14: comparing Sc on nano-particle concentration profiles

Table 1: The numerical values of $f''(0)$, $\theta'(0)$, $\phi'(0)$ for different values of temperature-dependent viscosity, $\gamma = G$..

$\gamma = G$	$f''(0)$	$\theta'(0)$	$\phi'(0)$
1.0	-0.88784	-0.36560	-2.11820
2.0	-0.69042	-0.37040	-2.12570
3.0	-0.58140	-0.37320	-2.12980
5.0	-0.46160	-0.37644	-2.13390
7.0	-0.39610	-0.37825	-2.13620

Table 1 displays the data for skin-friction coefficient, Nusselt number and Sherwood number corresponding to different values of temperature-dependent viscosity. The table reveals that an elevation in temperature-dependent viscosity leads to an increase in both the Nusselt number and Sherwood number, whereas the skin-friction coefficient experiences a decrease.

Table 2: The numerical values of $f''(0)$, $\theta'(0)$, $\phi'(0)$ for different values of temperature-dependent thermal conductivity, $\Omega = Ohm$.

$\Omega = Ohm$	$f''(0)$	$\theta'(0)$	$\phi'(0)$
1.0	-0.88784	-0.36560	-2.11820
2.0	-0.88954	-0.34922	-2.14060
3.0	-0.89048	-0.34046	-2.15240
5.0	-0.89140	-0.33140	-2.16470
7.0	-0.89180	-0.32678	-2.17100

Table 2 illustrates the relationship between the temperature-dependent thermal conductivity and the corresponding values of skin-friction coefficient, Nusselt number, and Sherwood number. The results indicate that as the temperature-dependent thermal conductivity increases, both the skin-friction coefficient and Sherwood number also increase, whereas the Nusselt number decreases.

CONCLUSION

The influence of the fluid parameters on the flow and heat transfer are investigated using graphs. From the graphs, an increase in temperature-dependent viscosity enhances the velocity profiles. The temperature profiles are increasing functions of temperature-dependent thermal conductivity. An increase in the nonlinear stretching parameters enhances velocity, temperature and nano-particle concentration profiles. The velocity profiles decrease with increasing values of magnetic field and permeability parameters. An increase in the Brownian motion parameters enhances temperature profiles and reduces nano-particle concentration profiles. An increase in the thermophoresis parameters leads to an increase in the temperature and nano-particle concentration profiles. The Prandtl numbers reduces the velocity and temperature profiles. The nano-particle concentration profiles are decreasing function of Schmidt number.

ORCID

Idongesit Fred Ekang https://orcid.org/0000-0002-4014-7635
Amos Oladele Popoola https://orcid.org/0000-0002-3376-9938

REFERENCES

Ayeni, R. O., Popoola, A. O., Omowaye, A. J. and Ayeni, O. B. (2009). “MHD flow and heat transfer of a viscous reacting fluid over a stretching sheet”, *Journal of the Nigerian Association of Mathematical Physics*, 15,1, pp. 485-490.

Crane, L. J. (1970). “Flow past a stretching plate”, *Z. Angew. Math. Phys*., 21, pp. 645-647.

Das, K. (2015). “Nanofluid flow over a nonlinear permeable stretching sheet with partial slip”, *J. of the Egyptian Math. Society*, 23, pp. 451-456.

Eid, M. R. and Mahny, K. L. (2017). “Unsteady MHD heat and mass transfer of a non- Newtonian nanofluid flow of a two-phase Model over a permeable stretching wall with heat generation/absorption”, *Advanced Powder Tech*., in press, doi:10.1016/j.apt.2017.09.021.

Ekang, I. F., Joshua, E. E. and Senge, I. O. (2022). “Casson fluid flow with heat generation and radiation effect through a porous medium of an exponentially shrinking sheet”, *World Journal of Applied Science and Technology*,14.1b, pp. 56-61. doi.org/10.4314/WOJAST.v14i1b.56.

Ekang, I. F., Joshua, E. E., Senge, I. O. and Nwachukwu, O. O. (2021). “MHD heat and mass flow of nano-fluid over a non-linear permeable stretching sheet”, *Journal of Mathematics and Computational Science*, 11,5, pp. 5196- 5212.

Gupta, P. S. and Gupta, A. S. (1977). “Heat and mass transfer on a stretching sheet with suction or blowing”, *Canad. J. Chem. Eng.*, 55, pp. 744-746.

Khan, W. A. and Pop, I. (2010). “Boundary layer flow of a nanofluid past a stretching sheet”, *Int. J. Heat Mass Transfer*, 53, pp. 2477-2483.

Oreyeni, T., Ramesh, K., Nayak, M. K. and Popoola, A. O. (2022). “Triple stratification impacts on an inclined hydromagnetic bioconvective flow of micropolar nanofluid with exponential space-based heat generation”, *Waves in Random and Complex Media*. doi: 10.1080/17455030.2022.2112994.

Oreyeni, T., Shah, N. A. and Popoola, A. O. (2022). “The significance of exponential space-based heat generation and variable thermophysical properties on the dynamics of Casson fluid over a stratified surface with non-uniform thickness”, *Waves in Random and Complex Media*. doi: 10.1080/17455030.2022.2119304.

Popoola, A. O., Baoku, I. G. and Olajuwon, B. I. (2016). “Heat and mass transfer on MHD viscoelastic fluid flow in the presence of thermal diffusion and chemical reaction”, *International Journal of Heat and Technology*, 34, 1, pp. 15-26.

Rana, P. and Bhargava, R. (2012). “Flow and heat transfer of a nanofluid over a nonlinearly stretching sheet: a numical study”, *Commun. Nonlinear Sci. Numer. Simul*., 17, pp. 212-226.

Sakiadis, B. C. (1961). “Boundary layer behaviour on continuous solid surfaces”, *AIChEJ*., 7, pp. 26-28.

Senge, I. O., Oghre, E. O. and Ekang, I. F. (2021). “Influence of radiation on magneto-hydrodynamics flow over an exponentially Stretching sheet embedded in a thermally stratified porous medium in the presence of heat source”, *Earthline J. of Math. Sci*., 5, 2, pp. 345-363.

Vajravelu, K. (2001). “Viscous flow over a nonlinearly stretching sheet”, *App. Math. Comput*., 124, pp.281-288.

Wang, C. Y. (2009). “Analysis of Viscous flow due to a stretching sheet with surface slip and suction”, *Nonlinear Anal. Real. World Appl*., 10, pp. 375-380.